Enhancing Au/TiO_2 Catalyst Thermostability and Coking Resistance with Alkyl Phosphonic-Acid Self-Assembled Monolayers

Alexander H. Jenkins, Charles B. Musgrave, J. Will Medlin*[+]

*Department of Chemical and Biological Engineering, University of Colorado Boulder, JSCBB D125, 3415 Colorado Avenue, Boulder, Colorado 80303, United States

[+]corresponding author: will.medlin@colorado.edu

ABSTRACT: Metal oxide-supported Au catalysts, particularly those with small Au nanoparticles, catalyze a variety of reactions including low-temperature CO oxidation and selective hydrogenation of alkynes. However, the facile nature of Au particle growth at even moderate temperatures poses significant challenges to maintaining catalyst activity under reaction conditions. Here, we present a method to reduce the rate of sintering and coke formation in TiO_2-supported Au catalysts via the deposition of alkyl-phosphonic acid (PA) self-assembled monolayers. After surface modification with PAs, the resultant catalysts exhibited significantly improved resistance to Au sintering. PA deposition strongly suppressed CO oxidation rates, consistent with poisoning of active sites. In contrast, modification with PAs significantly improved the rate of C_2H_2 hydrogenation on Au/TiO_2. The enhanced activity was accompanied by a dramatically improved resistance to accumulation of surface carbonaceous species.

KEYWORDS: *supported metal catalysts, self-assembled monolayers, thermostability, gold, acetylene hydrogenation, CO oxidation, interface, Ostwald ripening*

1. Introduction

Metal oxide-supported Au catalysts have received significant attention due to their unique catalytic properties. In 1987, Haruta et al. observed remarkably high activity for low-temperature CO oxidation on Au/TiO_2 catalysts.[1] They later showed that small Au nanoparticles (NPs) are considerably more catalytically active than larger ones due to the higher concentration of under-coordinated metal sites.[2] Since the identification of Au as a viable catalyst, Au-based catalysts have been demonstrated for a variety of reactions including acetylene (C_2H_2) hydrochlorination, low-temperature water-gas shift, and several chemoselective and partial hydrogenations.[3–5]

The necessity of maintaining small NPs for most Au-catalyzed applications presents significant challenges over the range of typical reaction conditions. When exposed to elevated temperatures, Au adatoms on the support become increasingly mobile, leading to NP sintering via Ostwald ripening.[6] Sintering of supported Au is facile compared to most other supported metal catalysts due to the weak binding of Au atoms to the support.[7,8] Au catalysts have been shown to sinter even at ambient temperature in the presence of certain reactants such as CO and O_2 that aid Au adatoms in diffusing across the support surface. As sintering progresses and the average Au NP size increases, the catalyst deactivates, typically irreversibly.[9]

In some systems, Au-catalyst deactivation has been attributed to catalyst poisoning via the formation of carbonaceous species, or coke. For instance, coke formation has been invoked to explain the rapid loss of activity in Au/TiO_2 catalysts used for semi-hydrogenation of alkynes.[10] Improving the stability of Au-based catalysts by reducing sintering and coke formation would not only mitigate the need to replace and regenerate the catalyst, but would also broaden the range of operating conditions under which these catalysts can be used.

While several methods have been demonstrated to improve the thermostability of supported Au, these strategies typically involve complex synthesis or the addition of expensive materials.[11–16] One particularly promising strategy by del Río et al. improved the sinter-resistance of Au/TiO_2 by depositing a partial monolayer of CeO_2 onto the existing catalyst in a single-step process.[17] They found that CeO_2 rafts interacted with Au to stabilize the NPs at temperatures up to 700°C. However, this work focused primarily on CO oxidation and did not address applicability at higher Au-loadings nor other factors of stability such as site-poisoning.

Here, we present a single-step method to reduce the rate of sintering and coke formation in Au/TiO_2 via the deposition of alkyl phosphonic acid (PA) self-assembled monolayers (SAMs). It has been previously shown that these PA SAMs selectively bind to metal-oxide support materials such as TiO_2 and Al_2O_3, while leaving Pt nanoparticles undecorated.[18–20] Thus, these SAMs can be added in excess to the catalyst to ensure full monolayer coverage without risk of covering metal NPs, which may not be the case for other NP stabilization strategies. Once present on the support, PA SAMs could potentially lower the rate of sintering by increasing the barrier for adatom diffusion across the support surface. However, the activity of interfacial metal sites at or near the support can be affected by these organic monolayers due to effects such as steric blocking of sites by the PA tail group, electronic modification of the surface, and the addition of acid functionality.[21,22] Because these interfacial sites at the perimeter

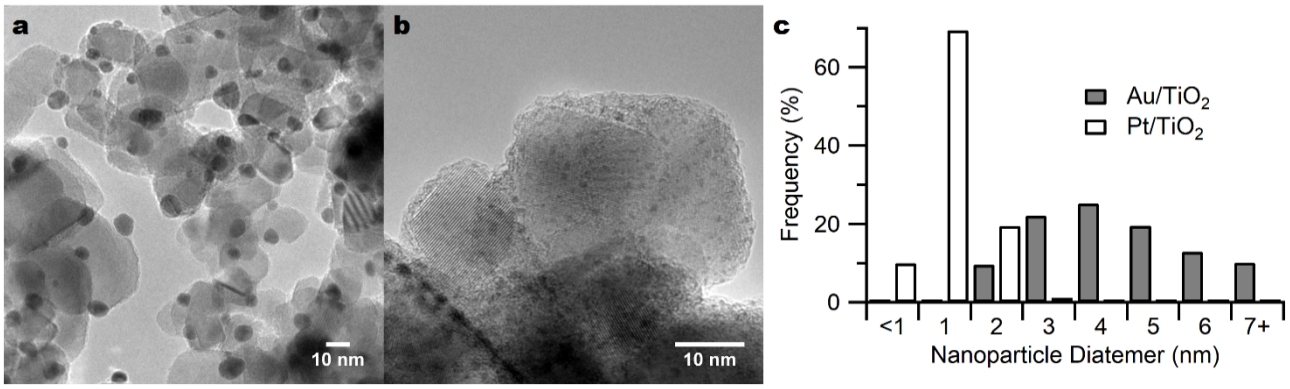

Figure 1. TEM images of synthesized (a) Au and (b) Pt nanoparticle catalysts supported on TiO_2. (c) Nanoparticle size histogram for Au (grey) and Pt (white).

of the NP are considered to be highly active for Au catalysts, we also studied the effects of PA SAMs on the catalytic behavior of Au/TiO_2 for two commercially relevant reactions: CO oxidation and acetylene partial hydrogenation.

One of the most notable catalytic uses of Au is in the low-temperature oxidation of CO to CO_2. Au-based catalysts have proved to be remarkably active for this reaction, making them a promising candidate for a number of applications including the removal of CO contaminants from H_2-rich streams.[23] The observed dependence of the reaction rate on Au particle size suggests that low-coordination Au atoms at the edges, corners, and metal-support interface play a key role in the adsorption and reaction of CO.[24–26] However, it has also been suggested We show here that by modifying Au/TiO_2 with PA SAMs we dramatically reduced the rate of Au NP sintering at elevated temperatures and decreased the rate of coke formation during acetylene hydrogenation. However, the SAMs also affected catalytic behavior at the Au-TiO_2 interface. Modification of Au/TiO_2 catalyst with PA SAMs caused a sharp decrease in catalytic activity for CO oxidation. Conversely, modification of Pt/TiO_2 with the same PAs resulted in much less deactivation for CO oxidation, consistent with prior reports that CO oxidation on Au-catalysts does occur primarily at the metal-support interface. In both systems the degree of deactivation correlated with the surface density of the PA monolayer. Additionally, we show that PA SAMs had a positive effect on acetylene hydrogenation activity on Au/TiO_2. This improvement in activity was partially due to a reduction of coke formation on PA-modified samples which led to a greater retention of catalyst activity during time-on-stream studies.

2. Experimental Section

2.1. Materials. Titanium (IV) oxide (Aeroxide® P25), chloroplatinic acid hexahydrate (A.C.S reagent), gold (III) chloride hydrate (99.999%), methylphosphonic acid (98%), butylphosphonic acid (98%), tert-butylphosphonic acid (98%), and phosphonoacetic acid (98%) were purchased from Sigma-Aldrich. Gold nanopowder (>99.95+%, 15 nm) was purchased from US Research Nanomaterials, Inc. High-performance liquid chromatography-grade tetrahydrofuran (THF, >99.9%) was purchased from OmniSolv. Acetylene (dissolved), 10% CO/He, and ultrahigh-purity H_2, O_2, and He, were obtained from Airgas. Urea (99%) was purchased from Fisher Scientific.

2.2. Catalyst Synthesis. Au/TiO_2 (7 wt%) was synthesized by the deposition-precipitation with urea (DPU7) method described by Zanella et al.[30] Pt/TiO_2 (8 wt%) was synthesized via incipient wetness impregnation as described by Üner et al.[31] Following preparation, the Au and Pt catalysts were calcined in air for 4 hours at 300°C and 400°C respectively. Crystallinity of the Au particles was further verified with X-ray powder diffraction (Figure S1). Phosphonate SAMs were deposited on the Au/TiO_2 and Pt/TiO_2 catalysts by liquid deposition in THF. Catalyst powder was added to a 10 mM solution of PA in THF and the resulting suspension was allowed to stir for 12 hours at ambient conditions. The solid was then separated by centrifugation in an Eppendorf 5804 centrifuge at 8000 rpm for 10 min and annealed at 120°C for 6 hours. The resulting solid was washed with THF and centrifuged three times (at 8000 rpm for 10 min), to remove any physisorbed PAs. The PA-modified powder was dried under vacuum at ambient temperature and the resulting catalysts were stored under refrigeration at 4°C.

2.3. Material Characterization. Transmission electron microscopy images were obtained using a Tecnai ST20 transmission electron microscope (TEM) equipped with a LaB_6 electron gun and low background single-tilt holder, and operated at 200kV. The average metal nanoparticle size and histogram of size distribution for each sample were established from the measurement of 300-500 particles from 3 separately prepared batches of catalyst. Standard deviations represent differences between catalyst batches. Dispersion was calculated based on the distribution of particle diameters with the approximation of hemispheric nanoparticles. Additional representative TEM images of all measured samples are shown in Figure S2. Additional high-magnification images and energy-dispersive X-ray spectroscopy (EDS) maps were obtained using an aberration corrected Thermo Scientific Titan Themis Scanning TEM

that the lack of an effect of the support material on catalytic behavior means interfacial Au atoms are not the main catalytic contributor for CO oxidation on supported Au.[27] By altering the support near this interface via PA SAMs, we can develop a further understanding of the reactivity of interfacial sites in this reaction.

Supported Au catalysts have been shown to selectively hydrogenate acetylene with minimal further hydrogenation to ethane, making them a promising candidate to purify ethylene streams.[28,29] However, Au-catalysts suffer from rapid loss of activity during acetylene hydrogenation, usually attributed to site poisoning via coke formation.[10]

equipped with an extreme field emission gun.

Fourier-transform infrared (FTIR) spectra were recorded using a Thermo Fisher Scientific Nicolet 6700 FTIR (100 scans at a resolution of 4 cm^{-1}). A closed cell attachment (Harrick) was used for diffuse reflectance infrared Fourier transform spectroscopy (DRIFTS). Spectra were collected in the hydrocarbon stretching region of 2700-3000 cm^{-1}.

Catalyst samples were also analyzed with an Optima 5300 inductively coupled optical emission spectrometer (ICP− OES) in order to determine their elemental compositions. PA SAM coverages and metal loadings were calculated from the data collected by this procedure.

2.4. Reactor Studies. CO oxidation, C_2H_2 hydrogenation, and temperature programmed oxidation (TPO) reactions were performed in a quartz tube, packed bed, continuous-flow reactor at atmospheric pressure. Prior to all reactions, catalyst was pretreated in 20% H_2 (balance He) at 150°C for Au and 200°C for Pt catalysts. For CO oxidation, a total flow rate of 50 sccm was used for 25 mg of catalyst. The feed mixture contained 1% CO, 20% O_2, and 79% He by volume. CO oxidation light-off curves were obtained by increasing the reactor temperature at a rate of 2°C/min. Acetylene hydrogenation reactions utilized 75 mg catalyst with a feed mixture containing 9% C_2H_2, 18% H_2, and balance He flowing at 55 sccm. TPO was performed on spent C_2H_2 hydrogenation catalyst using a 50 sccm stream of 20% O_2 in He, with temperature increasing at a rate of 10°C/min. Reactor effluent for CO oxidation and TPO reactions was measured using a Prisma™ 80 quadrupole mass spectrometer and for C_2H_2 hydrogenation using an Agilent Technologies 7890A gas chromatograph equipped with a 25 × 0.320 mm^2 Varian PoraPLOT Q capillary column and a flame ionization detector (split ratio = 25:1, column flow rate = 2 mL min^{-1}).

3. Results and Discussion

3.1. Catalyst Synthesis and Characterization. Au/TiO_2 and Pt/TiO_2 catalysts were synthesized via deposition-precipitation and incipient wetness impregnation, respectively. Through ICP-OES analysis it was determined that the metal loadings were 7 and 8 wt% for the Au- and Pt-catalysts, respectively. TEM was used to determine average nanoparticle size for both catalysts (Figures 1a and 1b). Figure 1c shows particle size distributions for the Au and Pt catalysts. Most Au NPs ranged from 3-7 nm in diameter and averaged 4.9 nm. Pt NPs were significantly smaller, ranging from 1-3 nm with an average diameter of 1.6 nm. Metal dispersion for the Au and Pt catalyst were estimated at 21% and 72%, respectively. The significant difference in NP size between Au and Pt was likely due to the different synthesis techniques used for each catalyst. Weaker binding of Au adatoms to the TiO_2 surface is thought to lead to greater Au mobility on the TiO_2 and thus increased ripening during the calcination step of synthesis.[7,32–35]

Table 1. Names, Abbreviations, Structures, and Surface Densities of PA Modifiers on Au/TiO_2

Modifier Name (abbreviation)	Structure	Surface Density (P/nm^2)
Methylphohsphonic Acid (MePA)	$CH_3PO(OH)_2$	5.2
n-Butylphosphonic Acid (nBuPA)	$CH_3(CH_2)_3PO(OH)_2$	4.6
t-Butylphosphonic Acid (tBuPA)	$(CH_3)_3CPO(OH)_2$	3.3

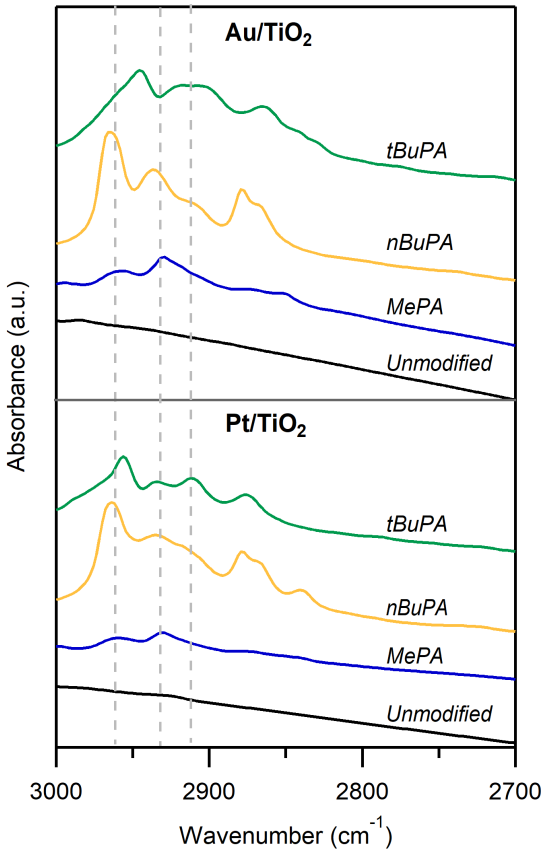

Figure 2. DRIFT spectra of PA-modified and unmodified Au/TiO_2 (top) and Pt/TiO_2 (bottom) catalysts.

Following the synthesis of Au/TiO_2 and Pt/TiO_2, a series of alkyl PA SAMs were deposited on both catalysts. Table 1 shows the structures and surface densities for each of the PA precursors as well as their surface densities as determined by ICP analysis. The PA surface density appears to decrease with increasing bulkiness of the alkyl tail. We note that the deposition of PA SAMs does not significantly affect the particle size distribution for these catalysts, as shown by TEM (Figure S3). Additional high-magnification images depicting the metal/support interface as well as EDS spectra of the MePA-modified Au/TiO_2 are shown in Figure S4.

DRIFT spectra of PA-modified Au/TiO_2 and Pt/TiO_2 were collected, as shown in Figure 2, in order to confirm the presence of the SAMs and characterize the C-H stretching modes. Peaks associated with C-H stretches were observed for all modified catalysts, while no such peaks were seen for the native catalysts.

For methylphosphonic acid- (MePA), n-butylphosphonic acid- (nBuPA), and tert-butylphosphonic acid- (tBuPA) modified catalysts, characteristic antisymmetric methyl stretching peaks were observed at ~ 2956 cm^{-1}, 2964 cm^{-1}, and 2952 cm^{-1}, respectively. Symmetric CH_3 stretching modes were observed in the 2870-2880 cm^{-1} range for all modified catalysts. Shifts in peak location between PAs were likely due to differences in the local environment for each PA modifier, and peak intensity was much greater for nBuPA and tBuPA SAMs due to the greater number of C-H bonds present. Both catalysts modified with nBuPA exhibited an asymmetric methylene stretching peak near 2933 cm^{-1}. The relatively high frequency of this peak signifies a disordered monolayer, common for short-chain alkyl ligands.[18]

It is possible to remove the alkyl tails from the PA-modified catalysts while retaining the phosphorous head-group through high-temperature oxidation. Heating the PA-modified catalysts to 350°C in air for 3 hours removed the PA tails, demonstrated by the absence of C-H stretching modes shown by DRIFTS (Figure S5). Degradation of the alkyl tails was further quantified with temperature-programmed oxidation (TPO) studies (Figure S6), where oxidation and removal of the tails peaked in the range of 350-425°C. ICP-OES showed that heat treatment at 850°C in air did not affect phosphorous loading.

Previous studies have demonstrated that PAs deposited with the method used in this study do not form significant coverages on Pt.[21] In order to determine whether PAs deposit onto Au in addition to the metal-oxide support, deposition of phosphonoacetic acid on a Au nanopowder was attempted. DRIFT spectra of this sample showed no peaks in the carboxyl stretching region of ~1720 cm^{-1}, indicating that the PAs failed to deposit onto the Au; in contrast, major peaks were observed from deposition on TiO_2 (Figure S7). However, EDS analysis of Au/TiO_2@MePA was inconclusive regarding the existence of PAs on supported Au; the P-Kα signal could not be resolved due to proximity to the Au-Mα peak (Figure S4). Thus, we cannot rule out that PAs may have bound to some Au sites, especially at the perimeters of Au nanoparticles due to altered electronic properties from metal-support interactions. We note that differences in catalyst synthesis methods between supported Au and the previously characterized supported Pt catalysts could contribute to changed tendency of PAs to modify the metal in addition to the support.

3.2. Au Nanoparticle Sintering. Thermal treatment was conducted on MePA-modified and unmodified Au/TiO_2 catalysts at 450°C in air for 4 hours. This treatment temperature falls near the typical light-off temperature for a catalytic converter on modern automobiles, as well as the required temperature for removal of coke via oxidation on Au-catalysts. Thermal treatment exceeded the required conditions for PA-tail removal, so any effect of the PAs was attributed to the phosphorous head group. Following treatment, the catalyst samples were analyzed with TEM to determine Au particle size distribution (Figure 3). Average NP sizes for the thermally treated Au/TiO_2 and Au/TiO_2@MePA were 7.2 and 4.9 nm, respectively, while estimated metal dispersion for these two catalysts were 21% and 15%. These changes represent a 47% increase in particle diameter and 29% decrease in Au dispersion following heat treatment on the unmodified catalyst while the PA-modified catalyst was essentially unchanged. Moreover, 32% of observed Au particles were greater than 8 nm in diameter in the thermally treated Au/TiO_2, compared to just 5% in the thermally treated PA-modified and untreated native catalysts.

Thermal treatment at 700°C in air was also conducted on MePA-modified and unmodified Au/TiO_2 catalysts. After 4 hours of treatment, average particle sizes of 5.9 and 8.0 nm were observed for the PA-modified and unmodified catalysts, respectively (Figure S8). Notably, the number of Au particles smaller than 5 nm decreased by 87% for the unmodified catalyst compared to just 34% for the PA-modified one. Thus, while moderate sintering occurred on the PA-modified catalyst at 700°C, it was to a significantly lesser degree than that on the native catalyst.

It is clear that modification with PA SAMs greatly improved resistance to sintering on Au/TiO_2 at elevated temperatures. Two main factors can contribute to a decrease in the rate of Ostwald ripening: a reduction in thermodynamic driving force and an increase in the kinetic barrier for adatom diffusion.[6] In this case, the latter factor seems more likely. Alghannam et al. showed in a first-principles study that Au adatoms migrated on the TiO_2 (101) surface with an activation energy of 0.24 eV, considerably lower than the barriers for Pt (0.84 eV) and Cu (1.23 eV). During this migration, Au adatoms "hopped" between OO bridge sites and 2-fold-coordinated oxygen anions.[32] In our experiments, the deposition of PAs on TiO_2 altered the geometry and coordination of surface oxygen atoms, likely leading to a more constrained adatom-migration pathway. Moreover, phosphates on the support would both sterically hinder Au adatoms from diffusing across the surface and compete with adatoms for adsorption sites.

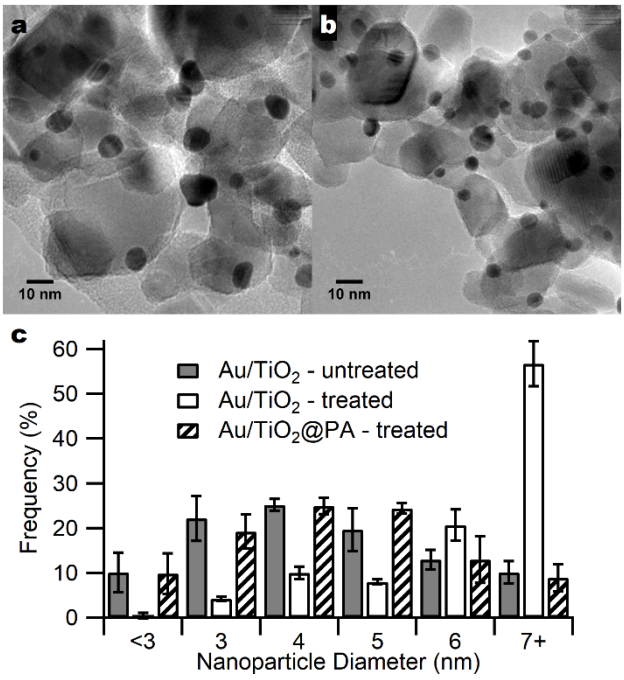

Figure 3. TEM images of thermally treated (a) unmodified and (b) PA-modified Au/TiO_2. (c) Nanoparticle size histogram for untreated Au/TiO_2, thermally treated Au/TiO_2, and thermally treated Au/TiO_2@PA. Thermally treated catalysts were heated to 450°C in air for 4 hours.

It is also possible that PA head groups at the metal-support

interface may interact with interfacial metal atoms in some systems to increase the coordination of interfacial atoms and thus lower the interfacial energy and resulting thermodynamic penalty for small NPs. If this is the case on Au/TiO_2, then the reduction in the thermodynamic driving force for Ostwald ripening would contribute to the lower rate of sintering.

3.3. CO Oxidation Studies. Although PA-modified catalysts appear to be more thermally stable, it is important to consider possible tradeoffs in activity due to occupation of $Au\text{-}TiO_2$ interface sites by the PAs as well as possible Au site blockage by adsorbed PAs. Gas-phase oxidation of CO was conducted in a tubular packed bed reactor over a temperature range of 30 - 350°C. Reactant feed stream composition and flow rate were held constant as the reactor temperature was ramped at a rate of 2°C/min. Light-off curves for the reaction on native and PA-modified Au/TiO_2 catalysts are shown in Figure 4a. The unmodified Au/TiO_2 catalyst was highly active at ambient temperature, converting over 75% of the CO at 30°C. CO oxidation on the PA-modified Au/TiO_2 was strongly suppressed, lighting off between 280 - 312°C. T_{50}, the temperature at which 50% CO conversion was reached, for each catalyst is shown in Table 2. For the PA-modified catalysts, the degree of catalyst deactivation increased with PA coverage density. This deactivation thus may be due to steric blocking or electronic modification of catalyst active sites (perhaps at the metal-support interface).

CO oxidation studies were also performed on PA-modified Au/TiO_2 after removing the PA alkyl tails *in-situ* through high-temperature oxidation. Shown with the dashed lines in Figure 4a, removal of the alkyl tail resulted in the recovery of some, but not all, catalytic activity. Once again, catalyst deactivation increased with PA coverage density. However, the degree to which each modified catalyst re-activated differed significantly. Following oxidation, the light-off temperature for tBuPA-modified Au/TiO_2 decreased by 165°C whereas the MePA-modified catalyst only saw a decrease of 43°C. Deactivation in the absence of alkyl tails may have been caused by phosphorous head-groups binding to oxygen anions on the TiO_2 surface, restricting the formation of surface hydroxyls and oxygen vacancies, both of which have been proposed as key components in O_2 activation.[25–27] Regardless of exact mechanism, the deactivation of CO oxidation on Au/TiO_2 with PA monolayers confirms the catalytic importance of interfacial sites for this system.

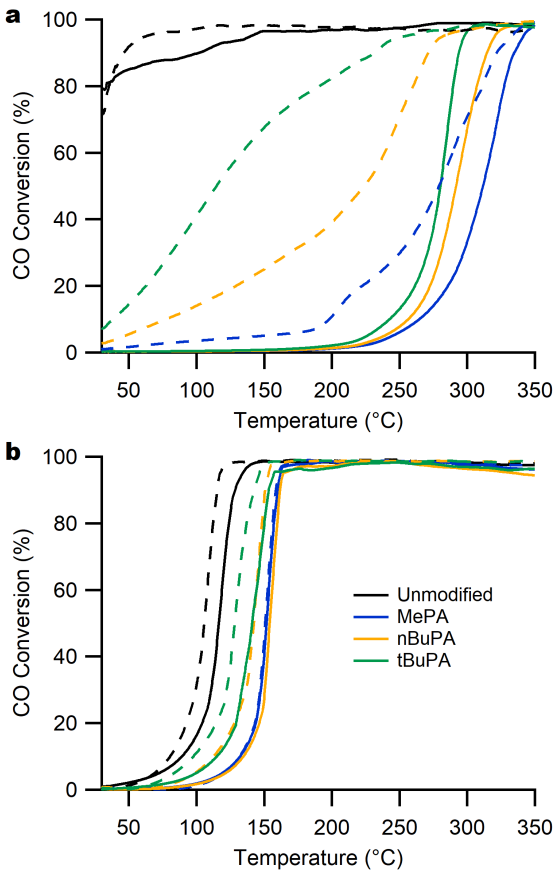

Figure 4. Light-off curves for CO oxidation on (a) Au/TiO_2 and (b) Pt/TiO_2. Catalytic activity was tested with (solid) and without (dashed) alkyl tails present on PAs. For the latter, alkyl tails were removed from PA SAMs via high-temperature oxi-

CO oxidation on Pt catalysts was performed identically to the previous experiments on Au/TiO_2. These experiments were done to determine the magnitude of the PA modification effects for a metal catalyst that is not thought to require interface sites for O_2 activation.[36,37] Light-off curves for the reaction on native and PA-modified Pt/TiO_2 catalysts are shown in Figure 4b. As expected, the native Pt/TiO_2 was inactive at ambient temperature and exhibited a light-off around 117°C. Following modification with PAs, light-off temperatures increased by less than 40°C (Table 2). Following tail removal via *in-situ* oxidation, the Pt catalysts experienced a slight gain in activity. However, the native Pt/TiO_2 catalyst saw a similar shift in light-off after high-temperature oxidation, suggesting that these improvements may be unrelated to the PA tails, but instead due to removal of some other species from the Pt surface. We note that mild deactivation of Pt/TiO_2 by PA head-groups could be due to electronic alteration of the interfacial metal sites or the blocking of O_2 dissociation pathways at the Pt-support interface.

Deactivation of Pt/TiO_2 by PA modification was far less dramatic than on Au/TiO_2. Because on Pt/TiO_2 only interfacial metal sites should be significantly affected by PA SAMs, this confirms the already widely accepted model of CO oxidation occurring on bulk Pt sites as opposed to relying heavily on interfacial sites. The improvement in catalyst stability provided by PA SAMs is far outweighed by the deactivation on Au/TiO_2, making PA-modified Au-catalysts a poor choice for low-temperature CO oxidation.

Table 2. T_{50} for CO oxidation on PA-modified Au- and Pt-TiO_2 catalysts

Catalyst	T_{50} (°C) – pre-oxidation	T_{50} (°C) – post-oxidation
Au/TiO_2	< 30	< 30
Au/TiO_2@MePA	312 ± 6.5	279 ± 11
Au/TiO_2@nBuPA	292 ± 2.9	244 ± 4.4
Au/TiO_2@tBuPA	280 ± 4.1	106 ± 6.7
Pt/TiO_2	117 ± 2.3	106 ± 2.4
Pt/TiO_2@MePA	152 ± 2.7	151 ± 1.9
Pt/TiO_2@nBuPA	154 ± 1.1	142 ± 2.4
Pt/TiO_2@tBuPA	141 ± 5.9	128 ± 5.1

3.4. Acetylene Hydrogenation Studies. While it has been frequently reported that the effectiveness of Au-based catalysts for acetylene hydrogenation is strongly dependent on NP size, few if any publications have suggested the Au-support interface as the primary active zone. Instead, this NP size dependence has been attributed to the greater ratio of edge and corner sites in smaller Au particles, as these under-coordinated sites dissociate H_2 more easily.[15,16] If the metal-support interface is not critical for this reaction, then PA SAMs should have little effect on catalyst activity while still enhancing stability against sintering. In this study, we modified Au/TiO_2 with PA SAMs and studied the effect of PA-modification on acetylene hydrogenation performance.

Gas-phase acetylene hydrogenation was conducted in a tubular packed bed reactor at 200°C. Acetylene conversion was kept low, as high conversion of this exothermic reaction can lead to localized overheating. Total C_2H_2 conversion and selectivity towards ethylene for both modified and unmodified Au/TiO_2 catalysts after 5 minutes on stream can be found in Figure 5a. At our reaction conditions, the unmodified Au/TiO_2 reached a conversion of approximately 6%. Modification with MePA, nBuPA, and tBuPA resulted in conversions of 13%, 8%, and 2%, respectively. Selectivity towards ethylene fell between 91-93% for all except the MePA-modified catalyst, which showed ~86% selectivity. Normalized conversion vs time-on-stream for the 90-minute experiments can be found for each catalyst in Figure 5b. A steady decrease in conversion over time was observed for the unmodified Au/TiO_2 case, while the modified catalysts saw no significant dip in activity over the 90 minutes.

The improvement in conversion seen in the MePA- and nBuPA-modified catalysts is likely a result of greater catalyst stability as opposed to lower hydrogenation barriers. The rapid deactivation of the unmodified catalyst makes comparison difficult, but it should be assumed that initial conversion on this catalyst was greater than that measured after 5 minutes on-stream. The tBuPA-modified catalyst showed enhanced stability on-stream but lower initial acetylene conversion than the native catalyst. While the explanation for this lower activity is not yet clear, it may be related to bulky tert-butyl tails blocking sites on the catalyst surface. The influence of PA SAMs on C_2H_2 hydrogenation activity indicates that the Au-TiO_2 interface takes part in this reaction, although the exact role of the interface remains unclear.

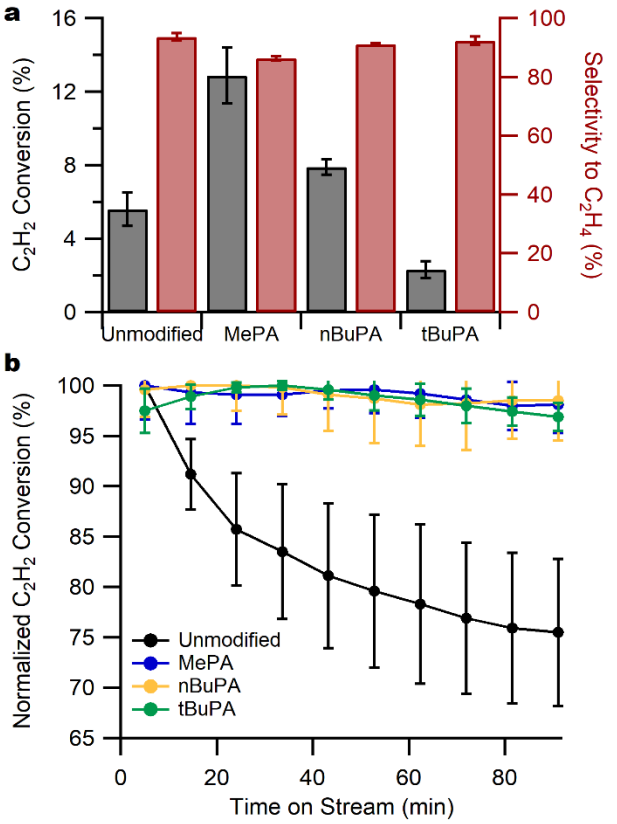

Figure 5. (a) C_2H_2 conversion (grey) and selectivity (red) for unmodified and PA-modified Au/TiO_2 after 5 minutes on-stream. (b) C_2H_2 conversion during on-stream hydrogenation, normalized for maximum observed conversion.

Activity loss during C_2H_2 hydrogenation on Au-catalysts has been previously reported and attributed to site-blocking via coke formation.[10,28] Coke formation was quantified with post-mortem TPO. During TPO, CO_2 production associated with the oxidation and removal of coke peaked at 325°C (Figure S6). TPO results (Figure 6) confirmed that the formation of coke on unmodified Au/TiO_2 greatly exceeded that on the PA-modified catalysts. On the native catalyst, 250 mg of carbon was removed for each gram of Au present. This is far greater than that for the PA-modified catalysts, for which carbon burn-offs ranging from 7-34 mg C/g Au were observed. Thus, we attribute the improved on-stream stability of the PA-modified catalysts to a dramatic reduction in poisoning by coke. This reduction in coke formation may be due to steric effects from the alkyl tails of the PAs mitigating the formation of larger hydrocarbons. To further confirm coke formation as the cause of activity loss in our unmodified Au/TiO_2, post-mortem DRIFTS experiments were run on each catalyst (Figure S9). Strong peaks in the C-H bonding region of 2700-3000 cm^{-1} showed the presence of hydrocarbons on the unmodified Au/TiO_2 catalyst. Differences in this region were significantly smaller for the PA-modified catalysts.

C_2H_2 hydrogenation was also conducted on each PA-modified Au-catalyst after removal of the alkyl tails via oxidation. Following tail-removal, conversion after 5 minutes on-stream increased for the nBuPA- and tBuPA-modified catalysts

to 14% and 8% respectively (Figure S10a). This significant increase in initial rate suggests that steric blocking by the alkyl tails was responsible for the lower activity of these samples compared to the MePA-modified catalyst. However, removal of these tails also resulted in a loss in catalyst stability. The activity of the oxidized samples dropped at a similar rate as the native Au/TiO_2 catalyst, indicating that the alkyl tails play a vital role in the suppression of coke formation (Figure S10b).

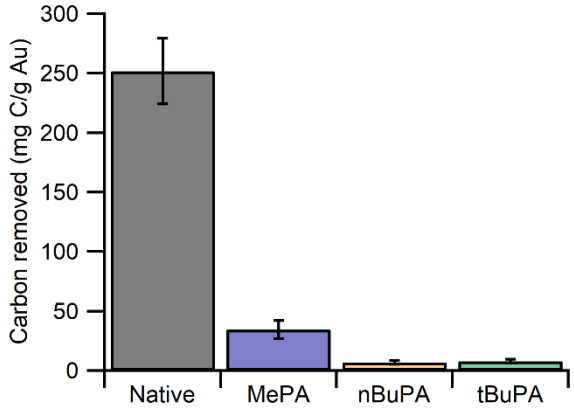

Figure 6. Carbon removed via oxidation of coke on PA-modified and unmodified Au/TiO_2 following 90 minutes of C_2H_2 hydrogenation

To demonstrate the effect of Au sintering on catalytic performance, C_2H_2 hydrogenation was also conducted on the catalysts thermally treated at 450°C (Figure S11). The unmodified Au/TiO_2 experienced a 43% loss in C_2H_2 conversion following heat treatment, while the PA-modified catalyst showed no change compared to un-treated catalysts with the same PA SAM. The 43% loss in activity despite just a 29% loss in Au dispersion on the unmodified catalyst is consistent with the assertion that low-coordination Au atoms are the primary sites for this reaction; the ratio of these low-coordination sites is inversely related to NP size.[23,24]

Overall, the modification of Au/TiO_2 with PA SAMs improved catalyst activity by reducing coke formation. This result, combined with the enhancement of catalyst stability by the reduction of NP sintering observed in PA-modified Au/TiO_2, suggests that PAs could play a useful role in the implementation of Au-catalysts for selective hydrogenation reactions.

4. Conclusions

Au/TiO_2 catalysts were modified with PA SAMs and tested for sintering resistance, CO oxidation activity, and C_2H_2 hydrogenation activity. The deposited PAs appeared to completely block sintering at 450°C over 4 hours whereas unmodified Au/TiO_2 saw an increase in average NP size of 47%. PA-modified Au- and Pt-catalysts experienced a loss in CO oxidation activity, likely due to modification of catalytic sites at the metal-support interface. This loss in activity was much more dramatic for Au/TiO_2, suggesting the importance of interfacial sites for CO oxidation on Au-catalysts. Acetylene hydrogenation activity increased on Au/TiO_2 following the deposition of MePA and nBuPA, partially due to a large reduction in catalyst poisoning via coke formation. Overall, the results reported here demonstrate that the deposition of PA SAMs significantly improved thermal stability and coke-resistance in Au/TiO_2. These PA-modified Au-catalysts appear especially well-suited for reactions at moderate temperatures under reducing conditions, such as C_2H_2 hydrogenation, where both sintering and coke formation are of concern. Moreover, the ability of PAs to bind to a wide variety of metal-oxide supports suggests that this method can extend to a large number of systems to improve catalyst stability.

Supporting Information

X-ray powder diffraction spectra for Au and Pt catalysts; Additional TEM images; Particle-size histograms for Au catalysts; High-magnification TEM and STEM-EDS images and spectra; DRIFT spectra for MePA-coated catalyst following tail removal; CO_2 production during TPO following C_2H_2 hydrogenation; DRIFT spectra of Au nanopowder following PA deposition; Particle size histogram for catalysts treated at 700°C; DRIFT spectra following C_2H_2 hydrogenation; C_2H_2 hydrogenation activity for PA-modified catalysts following tail-removal; C_2H_2 hydrogenation performance for thermally treated Au catalysts

Acknowledgments

This work was supported by the Department of Energy, Office of Science, Basic Energy Sciences Program, Chemical Sciences, Geosciences, and Biosciences Division [Grant No. DE-SC0005239]. AHJ acknowledges partial support from a Dept. of Education GAANN graduate fellowship. We also thank T. Van Cleve, S. Yazdi, M. Griffin, and J. Kenny for their assistance with measurements.

References

(1) Haruta, M.; Kobayashi, T.; Sano, H.; Yamada, N. Novel Gold Catalysts for the Oxidation of Carbon Monoxide at a Temperature Far Below 0 °C. *Chem. Lett.* **1987**, *16* (2), 405–408. https://doi.org/10.1246/cl.1987.405.

(2) Taketoshi, A.; Haruta, M. Size- and Structure-Specificity in Catalysis by Gold Clusters. *Chem. Lett.* **2014**, *43* (4), 380–387. https://doi.org/10.1246/cl.131232.

(3) Hutchings, G. J. Heterogeneous Gold Catalysis. *ACS Cent. Sci.* **2018**, *4* (9), 1095–1101. https://doi.org/10.1021/acscentsci.8b00306.

(4) McEwan, L.; Julius, M.; Roberts, S.; Fletcher, J. C. Q. A Review of the Use of Gold Catalysts in Selective Hydrogenation Reactions. *Gold Bull.* **2010**, *43* (4), 298–306. https://doi.org/10.1007/BF03214999.

(5) Fu, Q.; Weber, A.; Flytzani-Stephanopoulos, M. Nanostructured Au–CeO2 Catalysts for Low-Temperature Water–Gas Shift. *Catal. Letters* **2001**, *77* (1), 87–95. https://doi.org/10.1023/A:1012666128812.

(6) Ouyang, R.; Liu, J.; Li, W. Atomistic Theory of Ostwald Ripening and Disintegration of Supported Metal Particles under Reaction Conditions. *J. Am. Chem. Soc.* **2013**, *135* (5), 1760–1771. https://doi.org/10.1021/ja3087054.

(7) Wan, Q.; Hu, S.; Dai, J.; Chen, C.; Li, W. First-Principles Kinetic Study for Ostwald Ripening of Late Transition Metals on TiO2 (110). *J. Phys. Chem. C* **2019**, *123* (2), 1160–1169. https://doi.org/10.1021/acs.jpcc.8b08530.

(8) Hansen, T. W.; DeLaRiva, A. T.; Challa, S. R.; Datye, A. K. Sintering of Catalytic Nanoparticles: Particle Migration or Ostwald Ripening? *Acc. Chem. Res.* **2013**, *46* (8), 1720–1730. https://doi.org/10.1021/ar3002427.

(9) Yang, F.; Chen, M. S.; Goodman, D. W. Sintering of Au Particles Supported on TiO2 (110) during CO Oxidation. *J. Phys. Chem. C* **2009**, *113* (1), 254–260. https://doi.org/10.1021/jp807865w.

(10) Choudhary, T. V.; Sivadinarayana, C.; Datye, A. K.; Kumar, D.; Goodman, D. W. Acetylene Hydrogenation on Au-Based Catalysts. *Catal. Letters* **2003**, *86* (1–3), 1–8.

https://doi.org/10.1023/A:1022694505504.
(11) Zhu, H.; Ma, Z.; Overbury, S. H.; Dai, S. Rational Design of Gold Catalysts with Enhanced Thermal Stability: Post Modification of Au/TiO 2 by Amorphous SiO 2 Decoration. *Catal. Letters* **2007**, *116* (3–4), 128–135. https://doi.org/10.1007/s10562-007-9144-3.
(12) Manzorro, R.; Celín, W. E.; Pérez-Omil, J. A.; Calvino, J. J.; Trasobares, S. Improving the Activity and Stability of YSZ-Supported Gold Powder Catalyst by Means of Ultrathin, Coherent, Ceria Overlayers. Atomic Scale Structural Insights. *ACS Catal.* **2019**, *9* (6), 5157–5170. https://doi.org/10.1021/acscatal.8b04412.
(13) Arnal, P. M.; Comotti, M.; Schüth, F. High-Temperature-Stable Catalysts by Hollow Sphere Encapsulation. *Angew. Chemie - Int. Ed.* **2006**, *45* (48), 8224–8227. https://doi.org/10.1002/anie.200603507.
(14) Chen, C.; Shi, M.; Cargnello, M.; Fornasiero, P.; Murray, C. B.; Gorte, R. J. Au@TiO2 Core-Shell Nanostructures with High Thermal Stability. *Catal. Letters* **2014**, *144* (11), 1939–1945. https://doi.org/10.1007/s10562-014-1351-0.
(15) Zhao, K.; Qiao, B.; Wang, J.; Zhang, Y.; Zhang, T. A Highly Active and Sintering-Resistant Au/FeOx-Hydroxyapatite Catalyst for CO Oxidation. *Chem. Commun.* **2011**, *47* (6), 1779–1781. https://doi.org/10.1039/c0cc04171h.
(16) Wang, J.; Lu, A. H.; Li, M.; Zhang, W.; Chen, Y. S.; Tian, D. X.; Li, W. C. Thin Porous Alumina Sheets as Supports for Stabilizing Gold Nanoparticles. *ACS Nano* **2013**, *7* (6), 4902–4910. https://doi.org/10.1021/nn401446p.
(17) del Río, E.; Hungría, A. B.; Tinoco, M.; Manzorro, R.; Cauqui, M. A.; Calvino, J. J.; Pérez-Omil, J. A. CeO2-Modified Au/TiO2 Catalysts with Outstanding Stability under Harsh CO Oxidation Conditions. *Appl. Catal. B Environ.* **2016**, *197*, 86–94. https://doi.org/10.1016/j.apcatb.2016.04.037.
(18) Marshall, S. T.; O'Brien, M.; Oetter, B.; Corpuz, A.; Richards, R. M.; Schwartz, D. K.; Medlin, J. W. Controlled Selectivity for Palladium Catalysts Using Self-Assembled Monolayers. *Nat. Mater.* **2010**, *9* (10), 853–858. https://doi.org/10.1038/nmat2849.
(19) Schoenbaum, C. A.; Schwartz, D. K.; Medlin, J. W. Controlling the Surface Environment of Heterogeneous Catalysts Using Self-Assembled Monolayers. *Acc. Chem. Res.* **2014**, *47* (4), 1438–1445. https://doi.org/10.1021/ar500029y.
(20) Coan, P. D.; Griffin, M. B.; Ciesielski, P. N.; Medlin, J. W. Phosphonic Acid Modifiers for Enhancing Selective Hydrodeoxygenation over Pt Catalysts : The Role of the Catalyst Support. *J. Catal.* **2019**, *372*, 311–320. https://doi.org/10.1016/j.jcat.2019.03.011.
(21) Zhang, J.; Ellis, L. D.; Wang, B.; Dzara, M. J.; Sievers, C.; Pylypenko, S.; Nikolla, E.; Medlin, J. W. Control of Interfacial Acid–Metal Catalysis with Organic Monolayers. *Nat. Catal.* **2018**, *1* (2), 148–155. https://doi.org/10.1038/s41929-017-0019-8.
(22) Coan, P. D.; Ellis, L. D.; Griffin, M. B.; Schwartz, D. K.; Medlin, J. W. Enhancing Cooperativity in Bifunctional Acid–Pd Catalysts with Carboxylic Acid-Functionalized Organic Monolayers. *J. Phys. Chem. C* **2018**, *122* (12), 6637–6647. https://doi.org/10.1021/acs.jpcc.7b12442.
(23) Kung, M. C.; Davis, R. J.; Kung, H. H. Understanding Au-Catalyzed Low-Temperature CO Oxidation. *J. Phys. Chem.* **2007**, *111* (32), 11767–11775. https://doi.org/10.1021/jp072102i.
(24) Grunwaldt, J.; Baiker, A. Gold/Titania Interfaces and Their Role in Carbon Monoxide Oxidation. *J. Phys. Chem. B* **1999**, *103* (6), 1002–1012. https://doi.org/10.1021/jp983206j.
(25) Schubert, M. M.; Hackenberg, S.; van Veen, A. C.; Muhler, M.; Plzak, V.; Behm, R. J. CO Oxidation over Supported Gold Catalysts—"Inert" and "Active" Support Materials and Their Role for the Oxygen Supply during Reaction. *J. Catal.* **2001**, *197* (1), 113–122. https://doi.org/10.1006/jcat.2000.3069.
(26) Saavedra, J.; Doan, H. a.; Pursell, C. J.; Grabow, L. C.; Chandler, B. D. The Critical Role of Water at the Gold-Titania Interface in Catalytic CO Oxidation. *Science (80-.).* **2014**, *345* (6204), 1599–1602. https://doi.org/10.1126/science.1256018.
(27) Lopez, N.; Janssens, T. V. W.; Clausen, B. S.; Xu, Y.; Mavrikakis, M.; Bligaard, T.; Nørskov, J. K. On the Origin of the Catalytic Activity of Gold Nanoparticles for Low-Temperature CO Oxidation. *J. Catal.* **2004**, *223* (1), 232–235. https://doi.org/10.1016/j.jcat.2004.01.001.
(28) Gluhoi, A. C.; Bakker, J. W.; Nieuwenhuys, B. E. Gold, Still a Surprising Catalyst: Selective Hydrogenation of Acetylene to Ethylene over Au Nanoparticles. *Catal. Today* **2010**, *154* (1–2), 13–20. https://doi.org/10.1016/j.cattod.2010.02.021.
(29) Nikolaev, S. A.; Pichugina, D. A.; Mukhamedzyanova, D. F. Sites for the Selective Hydrogenation of Ethyne to Ethene on Supported NiO/Au Catalysts. *Gold Bull.* **2012**, *45* (4), 221–231. https://doi.org/10.1007/s13404-012-0066-5.
(30) Zanella, R.; Giorgio, S.; Henry, C. R.; Louis, C. Alternative Methods for the Preparation of Gold Nanoparticles Supported on TiO2. *J. Phys. Chem. B* **2002**, *106* (31), 7634–7642. https://doi.org/10.1021/jp0144810.
(31) Uner, D.; Tapan, N. A.; Özen, I.; Üner, M. Oxygen Adsorption on Pt/TiO2 Catalysts. *Appl. Catal. A Gen.* **2003**, *251* (2), 225–234. https://doi.org/10.1016/S0926-860X(03)00317-X.
(32) Alghannam, A.; Muhich, C. L.; Musgrave, C. B. Adatom Surface Diffusion of Catalytic Metals on the Anatase TiO2 (101) Surface. *Phys. Chem. Chem. Phys.* **2017**, *19* (6), 4541–4552. https://doi.org/10.1039/C6CP08789B.
(33) Sánchez-Sánchez, C.; Martín-Gago, J. A.; López, M. F. Small Pt Nanoparticles on the TiO2 (110)–(1×2) Surface. *Surf. Sci.* **2013**, *607*, 159–163. https://doi.org/10.1016/j.susc.2012.08.028.
(34) Gong, X.; Selloni, A.; Dulub, O.; Jacobson, P.; Diebold, U. Small Au and Pt Clusters at the Anatase TiO 2 (101) Surface: Behavior at Terraces, Steps, and Surface Oxygen Vacancies. *J. Am. Chem. Soc.* **2008**, *130* (1), 370–381. https://doi.org/10.1021/ja0773148.
(35) Mitchell, C. E. J.; Howard, A.; Carney, M.; Egdell, R. G. Direct Observation of Behaviour of Au Nanoclusters on TiO2(110) at Elevated Temperatures. *Surf. Sci.* **2001**, *490* (1–2), 196–210. https://doi.org/10.1016/S0039-6028(01)01333-4.
(36) Allian, A. D.; Takanabe, K.; Fujdala, K. L.; Hao, X.; Truex, T. J.; Cai, J.; Buda, C.; Neurock, M.; Iglesia, E. Chemisorption of CO and Mechanism of CO Oxidation on Supported Platinum Nanoclusters. *J. Am. Chem. Soc.* **2011**, *133* (12), 4498–4517. https://doi.org/10.1021/ja110073u.
(37) Berlowitz, P. J.; Peden, C. H. F.; Goodman, D. W. Kinetics of Carbon Monoxide Oxidation on Single-Crystal Palladium, Platinum, and Iridium. *J. Phys. Chem.* **1988**, *92* (18), 5213–5221. https://doi.org/10.1021/j100329a030.

TOC Graphic

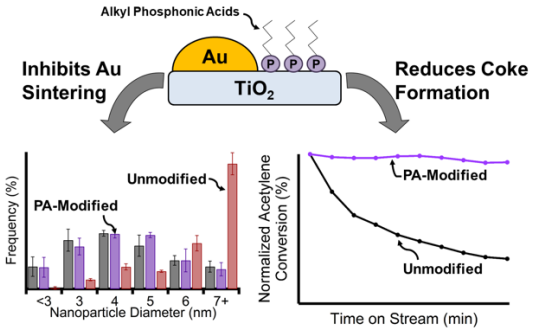
Alkyl Phosphonic Acids
Au
P
P
P
TiO2
Inhibits Au Sintering
Reduces Coke Formation
Unmodified
PA-Modified
Frequency (%)
<3
3
4
5
6
7+
Nanoparticle Diameter (nm)
PA-Modified
Unmodified
Normalized Acetylene Conversion (%)
Time on Stream (min)